FINAL PROJECT
REPORT #00042134-04-103
Volume III

GRANT: DTRT13-G-UTC45
Project Period: 10/1/2015 –6/1/16

FRP Reinforcement for Concrete: Performance Assessment and New Construction

Volume III: Construction and Monitoring of the Innovation Bridge

Participating Consortium Member:
University of Miami

Authors:
G. Claure, M. Rossini, T. Cadenazzi, C. Morales, O. Gooranorimi, S. Spadea, and A. Nanni

RE-CAST: Research on Concrete Applications For Sustainable Transportation
Tier 1 University Transportation Center

DISCLAIMER

TECHNICAL REPORT DOCUMENTATION PAGE

<table>
<tr><td colspan="2">Report No. RECAST UTC #00042134-04-103</td><td>2. Government Accession No.</td><td>3. Recipient's Catalog No.</td></tr>
<tr><td colspan="3">4. Title and Subtitle
FRP Reinforcement for Concrete: Performance Assessment and New Construction
Volume III: Construction and Monitoring of the Innovation Bridge</td><td>5. Report Date
August 3, 2016
6. Performing Organization Code:</td></tr>
<tr><td colspan="3">7. Author(s)
G. Claure, M. Rossini, T. Cadenazzi, C. Morales, O. Gooranorimi, S. Spadea, F. De Caso and A. Nanni</td><td>8. Performing Organization Report No.
Project #00042134-04-103</td></tr>
<tr><td colspan="3">9. Performing Organization Name and Address
RE-CAST - University of Miami
1251 Memorial Drive, Room 325
Coral Gables, FL 33146-0630</td><td>10. Work Unit No.
11. Contract or Grant No.
USDOT: DTRT13-G-UTC45</td></tr>
<tr><td colspan="3">12. Sponsoring Agency Name and Address
Office of the Assistant Secretary for Research and Technology
U.S. Department of Transportation
1200 New Jersey Avenue, SE
Washington, DC 20590</td><td>13. Type of Report and Period Covered:
Final Report
Period: 10/1/15 – 7/1/16
14. Sponsoring Agency Code:</td></tr>
<tr><td colspan="4">15. Supplementary Notes
NA</td></tr>
<tr><td colspan="4">16. Abstract
The University of Miami deliberately chose to construct a pedestrian bridge using concrete elements solely reinforced and prestressed with fiber-reinforced polymer (FRP) composites to demonstrate its commitment to innovation and sustainability. In addition to showcasing concrete reinforcing bars made of basalt and glass FRP (BFRP and GFRP), the bridge features unique BFRP forms such as continuous close stirrups used in the pier-caps and curbs as well as prefabricated BFRP cages for the auger-cast piles. The main load-carrying members of the bridge are two prestressed concrete girders of double-tee shape (as used in parking garage structures) with shortened flange overhangs. Each girder stem was prestressed with nine CFRP strands. Elements of the bridge were instrumented with vibrating-wire gages to monitor performance over time and during two load tests conducted on one of the prestressed concrete girders at the precast yard and on the completed structure, respectively. In addition to strain data, deflection measurements obtained during and after construction show field performance of the bridge to be in accordance with the predicted behavior.</td></tr>
<tr><td colspan="2">17. Key Words
Basalt fiber, bridge, carbon fiber, durability, fiber-reinforced polymer, glass fiber, prestressed concrete, reinforced concrete</td><td colspan="2">18. Distribution Statement
No restrictions. This document is available to the public.</td></tr>
<tr><td>19. Security Classification (of this report)
Unclassified</td><td>20. Security Classification (of this page)
Unclassified</td><td colspan="2">21. No of Pages
38</td></tr>
</table>

Form DOT F 1700.7 (8-72) Reproduction of form and completed page is authorized.

FRP REINFORCEMENT FOR CONCRETE: PERFORMANCE ASSESSMENT AND NEW CONSTRUCTION

VOLUME III: CONSTRUCTION AND MONITORING OF THE INNOVATION BRIDGE

PREPARED FOR THE

UNIVERSITY TRANSPORTATION CENTER

Written By:

Guillermo Claure[1], Marco Rossini[2], Thomas Cadenazzi[3], Carlos Morales[4], Omid Gooranorimi[5], Saverio Spadea[6], Francisco De Caso[7], and Antonio Nanni[8]

[1]Post-Doctoral Associate, Civil, Arch & Environ. Engineering
[2]Garduate Student, Civil, Arch & Environ. Engineering
[3]Graduate Student, Civil, Arch & Environ. Engineering
[4]Graduate Student, School of Architecture
[5]PhD Candidate, Civil, Arch & Environ. Engineering
[6]Fulbright Scholar, Civil, Arch & Environ. Engineering
[7]Research Asst. Professor, Civil, Arch & Environ. Engineering
[8]Professor and Chair of Civil, Arch & Environ. Engineering

UNIVERSITY OF MIAMI
RE-CAST

Submitted
August 3, 2016

FRP REINFORCEMENT FOR CONCRETE: PERFORMANCE ASSESSMENT AND NEW CONSTRUCTION

VOLUME III: CONSTRUCTION AND MONITORING OF THE INNOVATION BRIDGE

EXECUTIVE SUMMARY

Even though this pedestrian bridge named "Innovation Bridge" is a simple, single-span, 70 ft.-long construction, it offers a number of striking features intended to ensure a 75-year service life to its owner, the University of Miami. The bridge consists of the following concrete elements: auger-cast piles; cast-in-place pile caps and back walls; precast prestressed girders; and, cast-in-place deck topping and curbs.

This simple structure combines novel materials [Basalt-, Glass-, and Carbon-FRP (BFRP, GFRP and CFRP)] and novel composite manufacturing technologies (continuous close stirrups and preassembled cages) to ensure that degradation due to steel corrosion no longer undermines the longevity of the bridge. The eight, 16-in. diameter, 40 ft.-long auger-cast piles were reinforced with prefabricated cages made of six #6 BFRP rebars and spirals. The cages (in the shape of an octagon) were prefabricated at the BFRP manufacturer's plant and delivered to the site, ready for installation. The pile caps and back walls were built of concrete reinforced with straight bars, bent bars and close (continuous) stirrups made with BFRP and GFRP. The application of close BFRP stirrups takes advantage of performance efficiency of the composite reinforcement when continuity of the fibers is assured. The two prestressed girders have the shape of double-tees (as used in parking garage structures) with shortened flange overhangs. Each stem was prestressed with nine 0.6-in. diameter, seven-wire CFRP strands. Each tendon was tensioned to a load of 41.25 kip corresponding to 68% of its guaranteed capacity. The reinforcement grids for both stems and flange were made of pre-assembled interwoven BFRP bars (#3 and #4, respectively). Finally, the cast-in-place, 3-in. concrete deck topping was reinforced with a grid of BFRP bars (#3 in both directions). The reinforcement for the curbs consisted of a combination of close #4 BFRP stirrups (integral with the double-tee flange) and straight BFRP bars.

Reinforcing bars, tendons and concrete at various locations were instrumented with a total of 16 vibrating wire gages to allow for monitoring of the bridge elements over time and, in the case of the girders, during construction to measure effective strain and transfer length.

One of the two double-tees was load-tested at the precast yard with concentrated loads up to a maximum mid-span load of 27 kip (the girder remained un-cracked under this load). A second load test along with strain and deflection measurements was conducted after bridge completion to confirm expected structural behavior.

This project intended to demonstrate lower labor and equipment costs because of the reinforcement lightweight and pre-assembly. The expected low maintenance costs are the primary benefit to the owner.

ACKNOWLEDGMENTS

The authors gratefully acknowledge: a) the University Transportation Center "Research on Concrete; Applications for Sustainable Transportation (RE-CAST)" under grant US DOT, DTRT13-G-UTC45; b) the National Science Foundation (NSF) and its industrial members for the support provided to the Industry/University Center for Integration of Composites into Infrastructure (CICI) under grant NSF IIP-1439543; and, c) Infravation project "Sustainable Concrete Using Seawater, Salt-contaminated Aggregates, and Non-Corrosive Reinforcement (SEACON)".

The following participants and their roles in the project are also thankfully acknowledged:

OHL Arellano Construction Co. (General Contractor)
ANZAC Contractors, Inc. (Bridge Subcontractor)
Brill Rodriguez Salas & Associates, Inc. (Engineer of Record)
University of Miami (Architectural Design & Designated Engineer)
University of Miami - Structures and Materials Laboratory (Research Coordinator)
Coreslab Structures, Inc. (Double Tees Fabricator)
Tokyo Rope/Tokyo Rope USA (CFRP Manufacturer)
NO RUST REBAR, Inc. (BFRP Manufacturer)
Hughes Bros. (GFRP Manufacturer)
Titan America (Concrete Supplier)
MAPEI (Surface Products Supplier)

Findings and opinions expressed herein, however, are those of the authors alone and do not necessarily reflect the views of the sponsors.

TABLE OF CONTENTS

LIST OF FIGURES

1 INTRODUCTION

Conventional black steel reinforcing bars are made of steel with low carbon (C<0.2%). They are usually strengthened by controlled cooling immediately following hot rolling which produces a hardened outer layer and a ductile core. According to national and international standards, reinforcing steel bars fulfill several requirements regarding strength, ductility, bond to concrete, and weldability. As far as durability is concerned, steel bars are protected from corrosion when they are embedded in concrete, because an extremely thin oxide layer forms on their surface, which induces passivation (i.e., reduces the corrosion rate to negligible values). The protective passive film is promoted by the alkalinity of the solution present in the concrete pores that has a pH value around 13. Passivity may be lost when carbonation or a critical amount of chloride ions reach a bar surface (Bertolini et al. 2014). Protection of steel bars from corrosion for the expected service life is provided by the concrete cover. Chloride-induced corrosion, which occurs in reinforced concrete (RC) structures exposed to seawater or de-icing salts, is particularly critical because, once steel is depassivated, the corrosion attack progresses rather rapidly. Over time, chlorides penetrate through the concrete cover eventually reaching a critical threshold value. This threshold is rather variable, depending on several factors, but indicatively ranges from 0.4 to 1% by mass of cement for atmospheric exposure. After initiation, corrosion propagates in the form of localized pitting affecting serviceability and safety of the structure. RC durability is thus dependent on a concrete cover sufficiently thick and dense (i.e., resistant to chloride penetration).

An alternative strategy to attain durability of RC structures is to use reinforcement that is not susceptible to corrosion. Fiber reinforced polymer (FRP) bars are made of continuous fibers (basalt, carbon and glass) embedded in a polymeric resin matrix (vinyl ester and epoxy) via the pultrusion process or similar ones (Nanni et al. 2014). The fibers have the function of carrying the load; the resin has the function of binding together the fibers, transferring the load to the fibers, and protecting the fibers. As of today, glass is the most commonly used fiber for non-prestressed reinforcement with advantages such as high strength, low cost, high chemical resistance, and good insulating properties. Its drawbacks include low elastic modulus, sensitivity to abrasion, and low fatigue strength. Matrices are typically thermosetting resins with vinyl ester being the preferred one given its high mechanical toughness and excellent degradation resistance that coupled with ease of manufacturing makes it ideal for FRP pultruded systems. Conversely, carbon is the preferred fiber for FRP prestressing applications due to its insensitivity to creep-rupture.

Selection of proper fiber and resin is the key to ensure longevity of the FRP system. For this project, a combination of FRP products were used, namely: basalt fibers with epoxy resin and E-CR (Electrical/Chemical Resistant) glass with vinyl ester resin for the non prestressed reinforcement, and carbon fibers with epoxy resin for the seven-wire prestressing tendons.

The main factors affecting the characteristics of FRP elements are fiber volume, dimensional effects, rate of curing, manufacturing process, and quality control during manufacturing. The density of FRP bars is about one-fourth that of steel, which reduces transportation costs and makes the bars easy to handle at the job site. The tensile behavior of FRP is characterized by a stress-strain relationship, which is linear elastic up to failure. If compared to steel Grade 60 bars, basalt and glass FRP bars offer higher tensile strength, but lower ultimate tensile strain and lower tensile modulus of elasticity. Similarly, if compared to low-relaxation prestressing steel, carbon FRP exhibits similar stiffness and strength. Unlike steel, the tensile strength of a FRP bar varies with its diameter, while the longitudinal modulus does not change appreciably. This phenomenon is primarily due to the effects of shear lag. The mechanical properties of a FRP bar are influenced by

the environment. The presence of water, alkaline or acidic solutions, saline solutions, ultraviolet exposure and high temperature may affect the tensile and bond properties of basalt and glass FRP bars. For example, Mathieu and Benmokrane (2013) focused on durability of glass FRP bars when embedded in concrete and immersed in a saline solution. The objective was to simulate seawater environment and the effect of deicing salts for tests conducted on samples subjected to accelerated conditions. Comparing the results obtained for bars immersed in salt and tap water, the effects of these two different environments on glass FRP resulted not relevant. After 100 years (according to the Arrhenius model), the tensile strength retention should be in the range of 70-77%.

2 INNOVATION BRIDGE

Although this pedestrian bridge is a simple, single-span, 70 ft.-long construction, it offers a number of striking features intended to ensure a 75-year service life to its owner, the University of Miami (UM). The project was initiated in November 2015 with the order to proceed issued to the precast fabricator and completed in May 2016.

The bridge consists of the following concrete elements: auger-cast piles; cast-in-place pile caps, side blocks and back walls; precast prestressed girders; and, cast-in-place deck topping and curbs. Stainless steel is used for the bearing plates of the girders, the anchor bolts for the lampposts, and the railings. Even though this project initially specified the use of steel-strand prestressed concrete (PC) girders supported on traditional steel RC piles and pile-caps, UM deliberately chose to adopt the use of composites as internal reinforcement to demonstrate its commitment to innovation and sustainability for this pedestrian bridge used by students to access the sports and intermural fields on campus. As a result, there is not a single pound of “black steel” (carbon steel) in any element of the bridge; in fact, all reinforcement and tendons are made of FRP composites. In particular, the structure combines basalt FRP (BFRP), glass FRP (GFRP), carbon FRP (CFRP) and novel composite manufacturing technologies (continuous close stirrups and preassembled pile cages) to ensure that degradation due to steel corrosion no longer reduces the longevity of the bridge.

Reinforcing bars, prestressing tendons and concrete at various locations were instrumented with a total of 16 vibrating wire gages (VWGs) to allow for monitoring of the bridge elements over time and, in the case of the girders, during construction, to measure effective strains and transfer lengths.

Figure 1 shows a cross-section of the bridge over the pile cap. The drawing reports dimensions and some reinforcement details for the main elements of the structure that are presented and discussed in the photographs to follow according to the construction sequence. Appendix 1 illustrates in more detail the construction phases through a sequence of pictures taken on-site.

The RC and PC elements of the bridge were designed with consideration to existing guides and technical literature (AASHTO 2009; ACI 440.1R-15; ACI 440.4R-04; Nanni et al. 2014). However, deviations from the cited documents were necessary in order to accommodate and demonstrate advances in knowledge and technology. For example, the cited guides do not address the use of BFRP reinforcement, close stirrups and cast-in-place RC piles. FRP materials were characterized following specification available in the technical literature (FDOT dev932 and dev933; ICC-ES AC454 2016; ACI 440.3R-12).

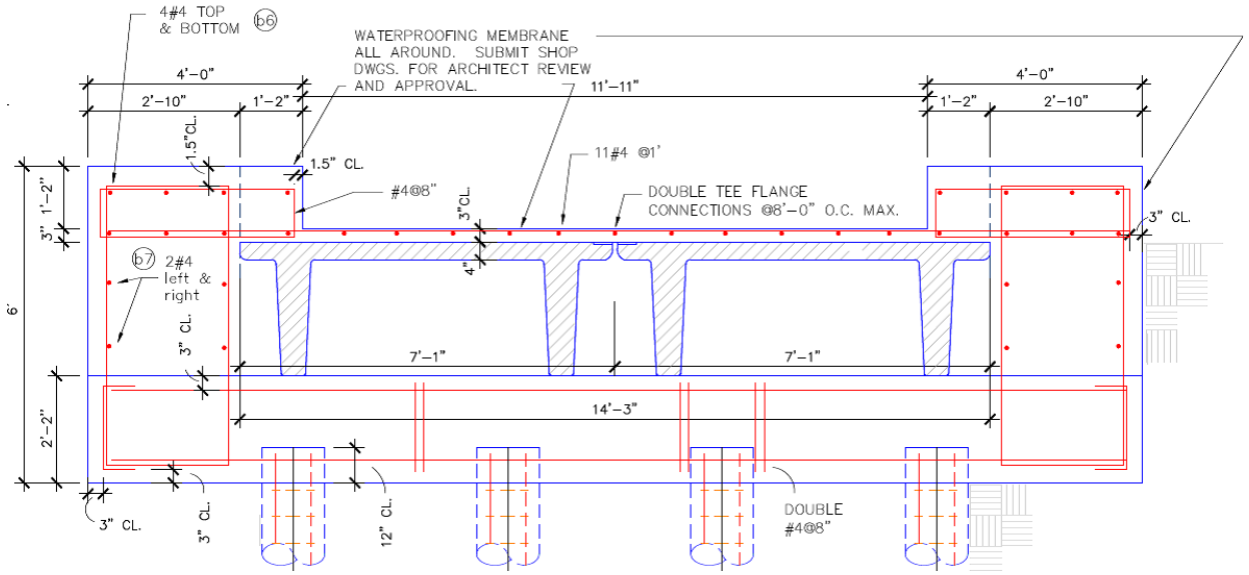

Figure 1: Bridge cross-section at pile cap

3 PRECAST PRESTRESSED DOUBLE-TEES

The two girders are in the shape of double-tees (typically used for parking garage structures) with shortened flange overhangs. Each stem was prestressed with nine 0.6-in. diameter, seven-wire CFRP strands. Each tendon was prestressed to a load of 41.25 kip corresponding to 68% of its guaranteed capacity. This value was intentionally higher of what presently suggested in ACI guidelines (ACI 440.4R-04).

CFRP tendons have been used for other prestressed or post-tensioned applications (Grace and Abdel-Sayed 1996), but never before with this diameter for the fabrication of double-tees (DTs) with thin cross-section stems. The prestressing of CFRP tendons remains a challenge due to the complexity of the anchor system that requires splicing with conventional steel strands.

The reinforcement grids for both stems and flange were made of pre-assembled interwoven BFRP bars (#3 and #4 at spacing 6 in. o.c., respectively). Figure 2 shows the casting bed for the two in-line DTs after the CFRP tendons were prestressed and all BFRP reinforcement was in place. Visible in the photograph are the continuous close stirrups to reinforce the curbs to be cast-in-place at the site. Also visible are two VWGs encapsulated in a protection shield and installed on the BFRP bars over the stem (longitudinal direction) and across the mid flange (transverse direction). The top insert is a close up view of the reinforcement over the stem while the self-consolidating concrete is being poured. Visible are: the top 7-wire CFRP strand; the supplemental top #7 BFRP bar over the stem; the BFRP top mat; and, the continuous close stirrup.

Figure 2: Double-tees casting bed and detail of BFRP reinforcement at casting

Figure 3 shows one of the DTs being lifted from the bed a day after casting. Visible are the nine plus nine CFRP tendon terminations and the continuous close stirrups for curb reinforcement. The red and blue cables connect the VWGs installed on tendons, reinforcing bars and concrete. The VWGs in the tendons helped confirming the degree of prestressing at tensioning and following stages.

Figure 3: Double-tee being lifted from the casting bed

The cross-section of the girder presenting location of strain gauges is shown in Figure 4. The schematic drawing illustrates the different type of strain gauges installed prior pre-casting and their location along the span length and with respect to the controller box installed on-site after conclusion of construction process. Appendix 2 presents a detailed report on the PC girders.

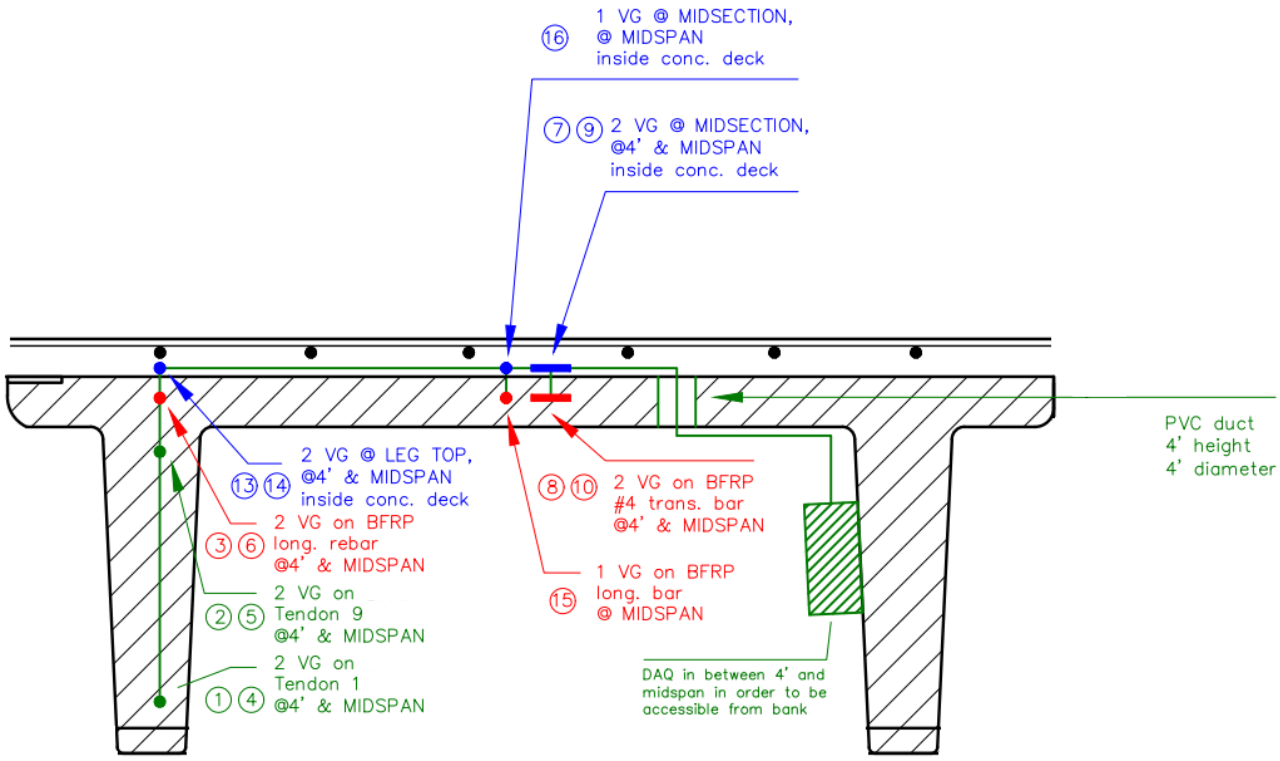

Figure 4: Double-tee cross-section and instrument locations

4 SITE CONSTRUCTION

The eight, 16-in. diameter, 40 foot-long auger-cast piles were reinforced with a prefabricated cage of six #6 BFRP bars and #3-equivalent BFRP spirals. The cages (in the shape of hexagons) were prefabricated at the composites manufacturer's plant and delivered to the site, ready for installation as shown in Figure 5. The factory prefabrication ensured high product precision and speed of on-site installation. Each cage was light enough to be picked up by two workers and moved without the use of any equipment. This application is a world "first" and takes advantage of precision manufacturing.

Figure 5: Delivery of BFRP pile cages at the site

The final phase of construction of one of the piles is shown in the photograph of Figure 6 where workers are seen pushing down into the grout-filled hole the last 5 feet of the reinforcement cage. Since the FRP weight is approximately one forth that of steel, the cage did not spontaneously sink in and workers had applied some direct force. This could have easily been done by using the scoop of the backhoe or by climbing onto the spiral as shown in the photograph. The latter was possible given the excellent chemical adhesion of the spiral to the longitudinal bars.

Figure 6: Construction of auger-cast pile

Figure 7 shows the termination of the four piles at one abutment with exposed reinforcement after grout removal. This operation was simple and did not cause any damage to the BFRP cage. Exposing the pile reinforcement was not a design requirement since conventional bridge practice for pinned pile connection to the cap simply requires the pile to be cut flush and extend one foot

into the cap. Exposing the reinforcement was selected to demonstrate the feasibility of the grout demolition process and the resilience of the FRP reinforcement. The red cable coming out of the second pile in the photograph connects to two VWGs installed on the pile longitudinal bars.

Figure 7: Exposed reinforcement in piles

The pile caps, side blocks (to support the lampposts) and back-walls are made of concrete reinforced with straight BFRP bars, bent GFRP bars and continuous close BFRP stirrups. The application of continuous close BFRP stirrups is a U.S. “first” which takes advantage of performance efficiency of the composite reinforcement when continuity of the fibers is assured. Because of their geometry, close stirrups do not require surface deformation to provide a mechanical bond to concrete. Additionally, the radius of curvature of the bend can be tighter as fibers need not slide over each other as required when bending a straight pultruded bar before the resin polymerizes. Figure 8 shows the completed assembly of the reinforcement cage for pile cap, side blocks and back-wall. The “U-shaped” deformed GFRP bars were used as the reinforcement for the back wall and were spliced into the deck reinforcement.

Figure 8: Reinforcement cage for pile cap, side blocks and back-wall

The installation of the second bridge girder is depicted in the photograph of Figure 9. Visible are the two neoprene rubber pads over the cap to provide contact with the stainless steel bearing plates mounted in each stem. Also visible is the back-wall reinforcement.

Figure 9: Installation of girder

The cast-in-place, 3-in. concrete deck topping was reinforced with a grid of BFRP bars (#3 at 8 in. spacing in both directions).

The reinforcement for the curbs consisted of a combination of close #4 BFRP stirrups (integral with the DT flange) and straight BFRP bars. Figure 10 shows the pouring of the 3-in. concrete

topping over the BFRP mat. Visible to the right are the stirrups for the curb reinforcement. In the foreground are the GFRP bars used to splice the back-wall U-shaped GFRP deformed reinforcement.

The blue and red cables connect the VWGs installed on the BFRP mat.

Figure 10: Casting of the deck topping

5 LOAD TESTS

5.1 Prestressed girder load test at pre-caster yard

Figure 11 presents the static load test of one of the two double-tees conducted 26 days after casting at the precast yard.

The simply supported girder was loaded with three concrete blocks at its mid-span for a total load of 27 kip plus self-weight. The total dead and live load corresponded to a maximum mid-span moment of 785 ft.-kip, which corresponded to 85% of the first-crack moment computed as 922 ft.-kip.

The results of the load test in terms of strains in the reinforcement and concrete and quarter-span/mid-span deflections measured with linear variable differential transformers (LVDTs) matched the analytical prediction. Appendix 2 provides detailed load test results.

Figure 11: Double-tee static load test at precast yard

5.2 Load test at completion of superstructure construction

Figure 12 shows the fully loaded pick-up truck used for the first field load tests. The total weight of the vehicle was 12,080 lb. with the heavier axle weighing 7,720 lb. The mid-span moment generated by the vehicle for load position one (maximum moment) including self-weight (i.e., two girders, decks and curbs) was equal to 1,402 ft.-kip, while the shear at the support for load position two (maximum shear) including self-weight was 84.8 kip. The bridge is designed for a distributed live load of 100 psf. Exceptional transit of a service vehicle is limited to 1,000 lb. wheel load.

Figure 12: Load test at completion of superstructure construction

Strains and deflections measured during the test were consistent with the analytical predictions. The strain in structural elements was recorded using VWGs attached to reinforcement. The strain in concrete and BFRP rebars were negligible while 30 micro-strain was recorded in one of the instrumented CFRP tendons. Additionally, no crack was observed in the bridge after the load test. Deflections are measured with a total station theodolite directed to permanently mounted targets on one of the exposed stem sides. Similar tests are planned at intervals of one year to monitor the bridge performance over time. Appendix 3 features a detailed report on deflection measurements at different stages of the research program.

6 BENEFITS AND BARRIERS

The primary expected benefit of this project is the low maintenance cost for the owner over the service life of the bridge. From a constructability perspective, FRP would allow reducing the deep concrete cover usually needed to ensure that degradation due to steel corrosion does not occur. Similarly, waterproof sealants and special concrete additives would no longer be necessary. Chloride contaminated concrete constituents: water (saltwater) and aggregates could be used without detrimental effects. This would include chloride-based accelerators and cement without chloride limits. Finally, FRP allows for lower labor and equipment costs because of the lightweight reinforcement handling and provides an opportunity for prefabrication of reinforcement cages with elimination field errors and overall better quality control.

Implementation of composites technology is, however, challenged by lack of consensus design protocols. Existing design guides are overly conservative and do not focus on performance, thus inhibiting a more rapid introduction of innovation. As the use of FRP becomes widespread, material costs higher than conventional steel will be easily offset by benefits of durability and ease of installation. Finally, FRP manufacturers and material suppliers have not yet created a reliable and respectable industry with the ability to speak as one voice and ensure stringent quality control of its products. This is perhaps the most critical shortcoming at the moment to generate the necessary confidence in owners, designers and contractors.

7 CONCLUSIONS

After almost three decades from its first commercial applications, RC and PC construction with FRP reinforcement is finally at the dawn of widespread acceptance and use as perhaps the most suitable response to the durability challenges of concrete construction.

The opportunities offered by composites are certainly not limited to improved durability; it can be argued that innovations in reinforcement forms, fabrication and delivery can elevate the quality, constructability and performance of concrete construction.

This is not just an option to make RC and PC more competitive technologies, it is a social responsibility in order to address the challenges related to sustainability.

8 REFERENCES

AASHTO (2009), LRFD Bridge Design Guide Specifications for GFRP Reinforced Concrete Bridge Decks and Traffic Railings, American Association of State Highway and Transportation Officials (AASHTO), Washington, DC

ACI 440.1R-15 (2015), Guide for the Design and Construction of Structural Concrete Reinforced with Fiber-Reinforced Polymer Bars, American Concrete Institute, Farmington Hills, MI

ACI 440.3R-12 (2012), Guide Test Methods for Fiber-Reinforced Polymers (FRPs) for Reinforcing or Strengthening Concrete Structures, American Concrete Institute, Farmington Hills, MI

ACI 440.4R-04 (Reapproved 2011), Prestressing Concrete Structures with FRP Tendons, American Concrete Institute, Farmington Hills, MI

Bertolini, L., Elsener, B., Pedeferri, P., Redaelli, E., Polder, R. (2014), "Corrosion of Steel in Concrete – Prevention, Diagnosis, Repair", 2nd edition, Wiley-VCH, 978-3-527-33146-8, 414

FDOT dev932 (2016), Florida Department of Transportation Developmental Specifications for Nonmetallic Accessory Materials for Concrete Pavement and Concrete Structures, Tallahassee, FL

FDOT dev933 (21016), Florida Department of Transportation Developmental Specifications for Installation of Fiber Reinforced Polymer Prestressing Strand in Concrete Structures, Tallahassee, FL

Grace, N. F., and Abdel-Sayed, G. (1996), "Double Tee and CFRP/GFRP Bridge System," Concrete International, 18 (2), 39-44

ICC-ES (2016), AC454 - Acceptance Criteria for Fiber-Reinforced Polymer (FRP) Bars for Internal Reinforcement of Concrete and Masonry Members, International Code Council - Evaluation Service, Inc., Los Angeles, CA

Mathieu, R. and Benmokrane, B. (2013), "Combined Effects of Saline Solution and Moist Concrete on Long-term Durability of GFRP Reinforcing Bars," Construction and Building Materials, 38, 274-284

Nanni, A., De Luca, A., Jawaheri Zadeh, H. (2014) "FRP Reinforced Concrete Structures – Theory, Design and Practice," CRC Press, 978-0-415-77882-4, 397

APPENDIX 1 – Construction Process

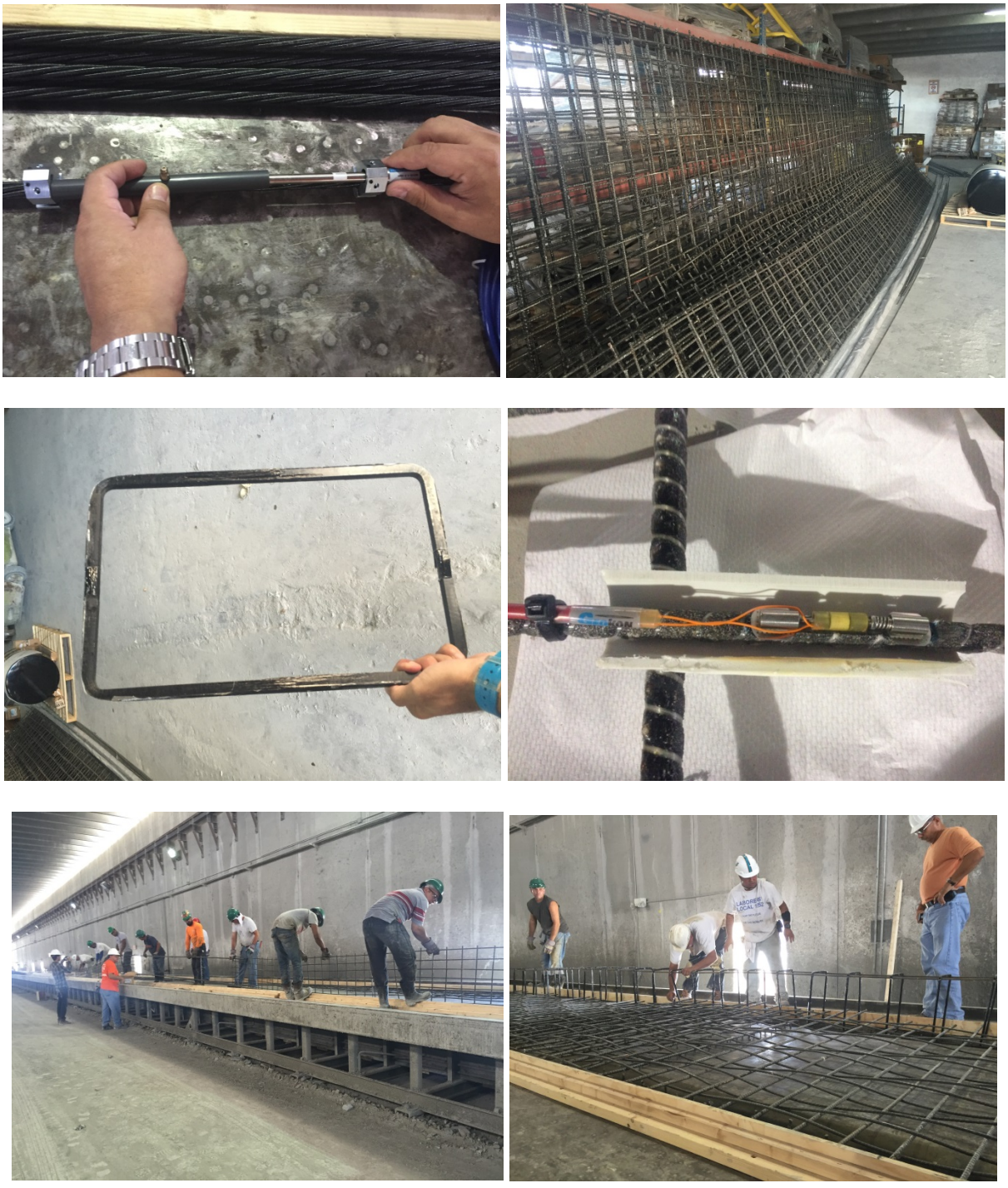

PC girder instrumentation and construction

Pile cap preparation, girder setup, and deck instrumentation and construction

Deck and curbs casting, and railing installation

APPENDIX 2 – CFRP Prestressed Girders

1. Introduction

The design of CFRP PC elements is generally based on the assumptions traditionally adopted for steel PC concrete. The most peculiar aspects to be carefully considered are: the brittle nature of the CFRP strands, their long-term behavior under sustained loads, and their bond-to-concrete properties.

ACI 440.4R suggests to reduce the maximum allowable tensioning stress at tensioning in CFRP tendons using a 0.65 safety factor to prevent undesired sudden failures. In addition, a proper environmental reduction factor has to be adopted for CFRP composites (ACI 440.1R) to take into account for long-term exposure to the environment.

Two major challenges to address are:

1) Fully exploit the mechanical properties of the CFRP strands; and,
2) Applying the CFRP prestressing technology to thin walled concrete section.

2. Materials and Design

2.1. CFCC

Carbon fiber composite cable (CFCC) manufactured by Tokyo Rope Manufacturing Co. Ltd., Japan, was the tendon type used in this study. This class of reinforcement is of interest to the Florida Department of Transportation and other DOTs for use as a corrosion-resistant reinforcing material for prestressed precast-concrete bridge superstructure (beams and deck) and substructure (piles and sheet piles) applications. CFRP strands have higher tensile fatigue resistance than PC steel strands and similar relaxation ratio. CFRP creep elongation is smaller than that of other FRP materials such as GFRP and aramid FRP, and equal to steel cables.

CFCC is a stranded cable comprising a number of individual rods (wires). In general, these cables are made with 7, 19, or 37 counter-clockwise twisted carbon rods, with nominal diameters varying from 0.2 to 1.6 in. Individual rods of CFCC consist of carbon fibers impregnated with thermosetting epoxy resin. In addition, each rod is protected with wrapping material (polyester fiber).

This study involved CFCC seven-wire cables, with a 0.179 in^2 cross-sectional area. The mechanical properties obtained by the material characterization on the CFCC cables are reported in Table 1, together with the values exhibited by conventional low relaxation steel strands having similar geometrical characteristics. The data show how CFCC may be considered a pre-stressing material even more efficient than traditional high-strength steel because of its high breaking load and lower modulus of elasticity. The high breaking load allows high pre-stressing rate whereas the lower elastic modulus causes reduced losses resulting from elastic shortening and creep of concrete. The nominal failure capacity guaranteed by Tokyo Rope is 60.7 kip, a value is similar to the steel cable capacity.

Table 1

Material	*Nominal Diameter*	*Area*	*Breaking Load (Guaranteed breaking load)*	*Elastic Modulus*
	(in.)	*(in^2)*	*(kip)*	*(msi)*
CFCC (1x7)	0.6	0.179	83.1 (60.7)	21.6
PC Steel (1x7)	0.6	0.217	61.2	28.7

2.2. Concrete

A self-compacting concrete (SCC) with specified compressive strength of 6,000 psi, supplied by Titan America, was employed in this work. The measured air content and spread of the fresh mix were respectively 1.0% and 25 in. The average compressive strengths, measured at different times, are reported in Table 2. The compressive test results were used to determine the tensile strength of the concrete and its modulus of elasticity at different stages. The ACI 318 (2014) correlation formulae, together with the Florida DOT aggregate characterization factor, were used.

Table 2

Time (# of samples)	*24 h (1)*	*7 days (3)*	*28 days (3)*	*75 Years*
Compressive Strength (psi)	5,307	7,335	8,068	8,668
Tensile Strength (psi)	546	642	674	698
Modulus of elasticity (ksi)	3,599	4,232	4,438	4,600

2.3. Design

The design of the DT girders presented in this work involves two major challenges:

1) Tensioning the cables up to the 68% limit instead of the 65% threshold imposed by (ACI 440.4R);

2) Applying the CFRP technology to DT sections, taking advantage of the extraordinary possibilities offered by SCC in achieving daring shapes.

The cross-section of a DT girder is shown in Figure 1, while Figure 2 partially shows the top view of the girder. The total depth of the precast section is 30 in., with a flange thickness of 4 in. The total width of the flange is 7¼ in. at the top and 6 in. at the bottom. The length of the girders is 68 ft 8 in., with the clear span being 66 ft. The girders are aimed to be completed on-site with a 3 in. topping and, on one side, with a 14 in. x 14 in. curb, both cast with a 4,500 psi specified strength concrete. Since the DTs need to be installed in parallel, the curb is supposed to be cast on a different side for the two girders. Each stem of the DTs includes nine CFRP (1x7 15.2Ø) tendons, tensioned with an initial prestressing force of 41.25 kip per strand before losses. Hence, a total tensile force of about 370 kip with a 10.7 in. eccentricity is intended to be applied to each of the DT stems.

A “safety” #7 BFRP bar is also positioned at the end each span. In addition, the reinforcement consists of two BFRP reinforcing meshes. The first mesh is acting as longitudinal (#4 @ 6 in.) and transverse reinforcement (#4 @ 6 in.) in the flange. The second mesh (#3 @ 4 in. longitudinal and #3 @ 6 in. transversal direction) is placed on both sides of the CFRP in the stems to reinforce the transfer-length region of the stems. Finally, #4 BFRP closed stirrups were partially embedded on one side of the flange of both DTs, to act as transverse reinforcement in the concrete curbs.

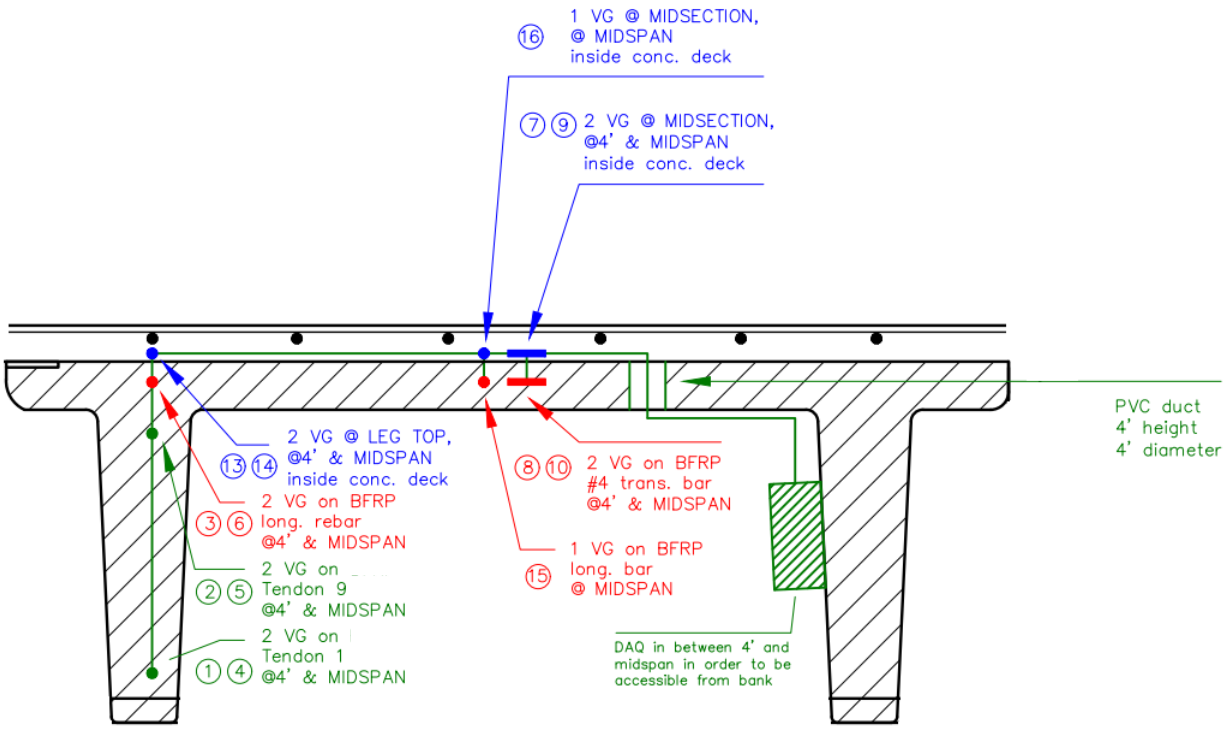

Figure 1: Cross-section of the DT girder

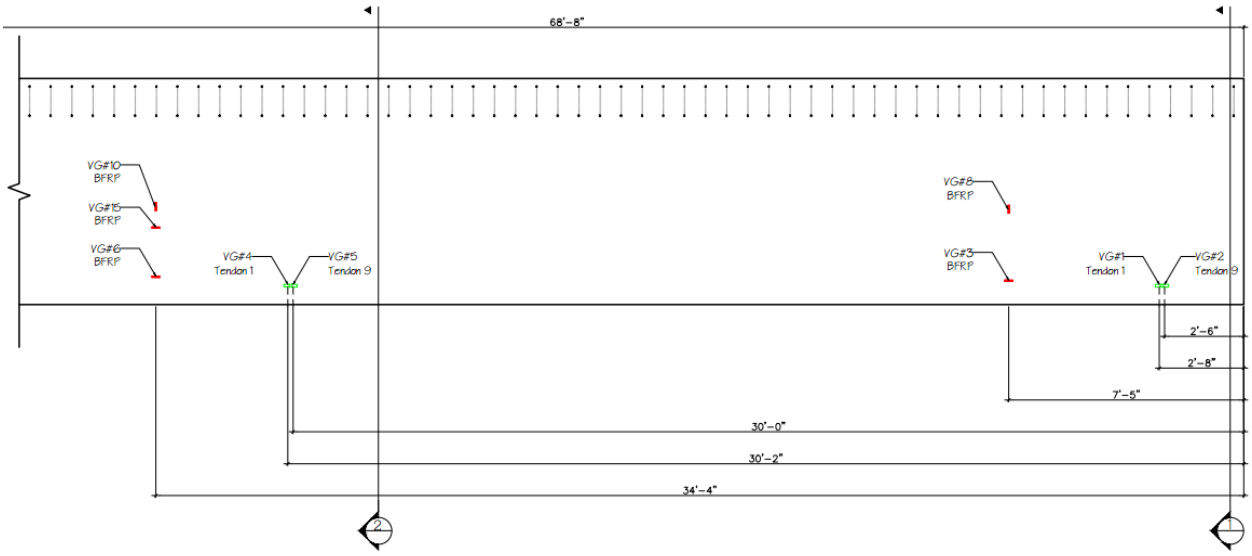

Figure 2: Plan of the DT girder

Table 3 shows the nominal flexural capacity and cracking moment calculated considering: 1) the precast DT section at 28 days; and, 2) the precast DT section completed with the concrete topping at a 75-year service life. A step-by-step analytical procedure based on a semi-analytical model was employed to take into account for concrete creep and shrinkage of the pre-cast DTs. Relaxation and creep of CFCC were modelled using two different logarithmic laws based on extrapolation of experimental data given by the producer.

Table 3

	28 days (girder only)	*75 years (with topping)*
Flexural Capacity (kip-ft)	2159	2644
Cracking Moment (kip-ft)	634	950

3. Construction

Two DT precast girders were constructed and instrumented at the Coreslab plant of Miami, adopting a pre-stressing bed and equipment available for conventional DT girders. CFRP strands and the BFRP reinforcement were arranged and positioned before the CFRP tensioning phases took places (Figure 3).

Figure 3: BFRP reinforcement and CFRP tendons arranged in the Coreslab prestressing bed

3.1. Instrumentation

With the aim of monitoring the strains during its entire service life, one of the two girders was instrumented with nine vibrating gauges, four installed on the CFRP tendons and five installed on the BFRP reinforcement (Figure 2).

As shown in Figure 2, the top (T9) and the bottom (T1) tendons of a selected stem were taken into consideration: two gauges were installed at DT midspan (VG4 and VG5, respectively), whereas two of them were installed at about 3 ft from a selected support (VG1 and VG2, respectively). Similarly, VG6 and VG3 were installed on the BFRP longitudinal reinforcement in correspondence of the monitored stem, at DT midspan and at 3 ft from the support, respectively. VG15 was installed on the BFRP reinforcement, in the middle of the deck, at DT midspan. VG10 and VG8 were installed on the transverse BFRP reinforcement, in the middle of the deck, at DT midspan and at 3 ft from the support, respectively.

3.2. Tensioning

Since CFRP is a brittle material, particular attention was paid to the tensioning and releasing phases. The prestressing force was applied to equivalent steel cables (See Table 1), using a hydraulic jack powered by a pump. The tensioning force of 41.25 kip was measured using a calibrated pressure transducer and verified by both measuring the cables elongation and monitoring the strains in the instrumented tendons. The load applied at jacks corresponds to a stress level of approximately 68% of the ultimate guaranteed capacity of CFRP (See Table 4).

The CFRP strands were attached to steel cables with a proprietary mechanical anchorage system to facilitate pulling of the strands without damaging their ends. This anchorage system consisted of sleeve for CFRP, wedges, joint coupler, mesh sheet, braided grip, and wedges for attaching the steel strand. Figure 4 shows the anchorage system for CFRP strands. After prestressing the strands, SCC was poured (Figure 5).

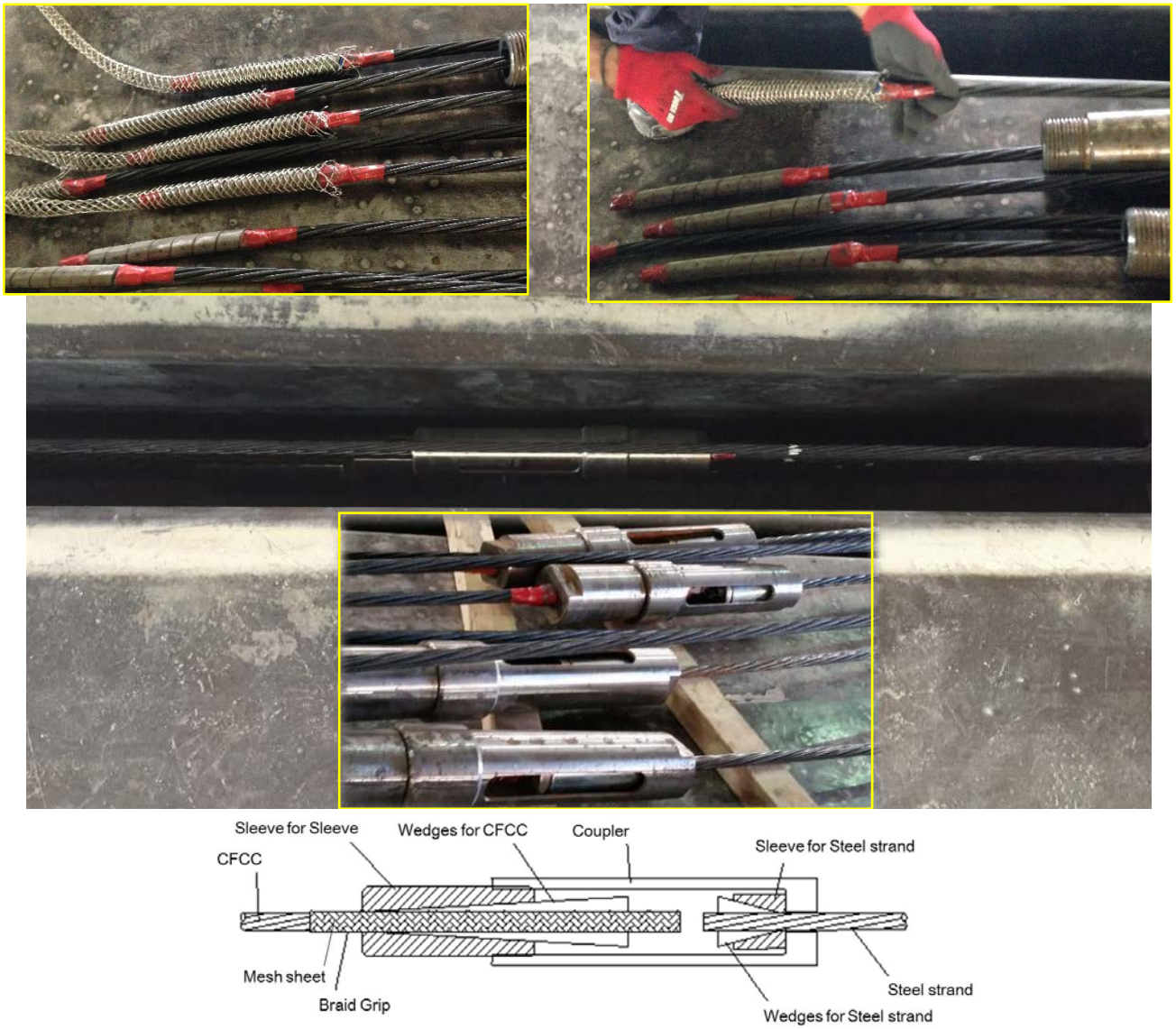

Figure 4: CFCC strand anchorage system

Figure 5: Concrete pouring phase

3.3. Releasing

The release of the prestressing forces took place 24 hours after casting. At that time, the concrete compressive strength was 5,347 psi. The pretensioned CFRP strands were cut in the middle of the bed while, at the same time, the steel cables were cut at both ends of the DT girders. Following this operation, the girders were successively demolded (Figure 6).

Figure 7 shows the strain measurements performed on the top and bottom tendons: a) after the tensioning phases (0 hours); b) after the concrete pouring (6 hours); c) after the release of prestressing forces (24 hours); and, d) after the demolding and complete curing of the PC girders (28 days). The first strain loss (b-a) deals with the pretensioning apparatus settlement (i.e., CFRP and steel cables anchorage systems). The second loss (c-b) is due to the elastic shortening of concrete at the time of the release. The third loss is caused by concrete creep/CFRP relaxation during the 28 days of curing.

The strains measured at midspan of the tendons (VG4 and VG5) are in line with preliminary calculation and theoretical prediction. The strain measurements performed near the supports (VG1-VG2 average) show, as expected, the progressive loss of bond of the tendons given the gages location within the development length zone.

The average prestressing force immediately following transfer is 38.1 kip and corresponds to a stress level of approximately 63% of the ultimate guaranteed capacity of CFRP (See Table 4).

Table 4

	ACI 440.4R Limitation	*Current Application*	*Registered Increment*
Applied load to guaranteed capacity ratio at jacking	0.65 f_{fu}	0.68 f_{fu}	+4.6%
Applied load to guaranteed capacity ratio immediately following transfer	0.60 f_{fu}	0.63 f_{fu}	+5%

Figure 6: Girders demolding

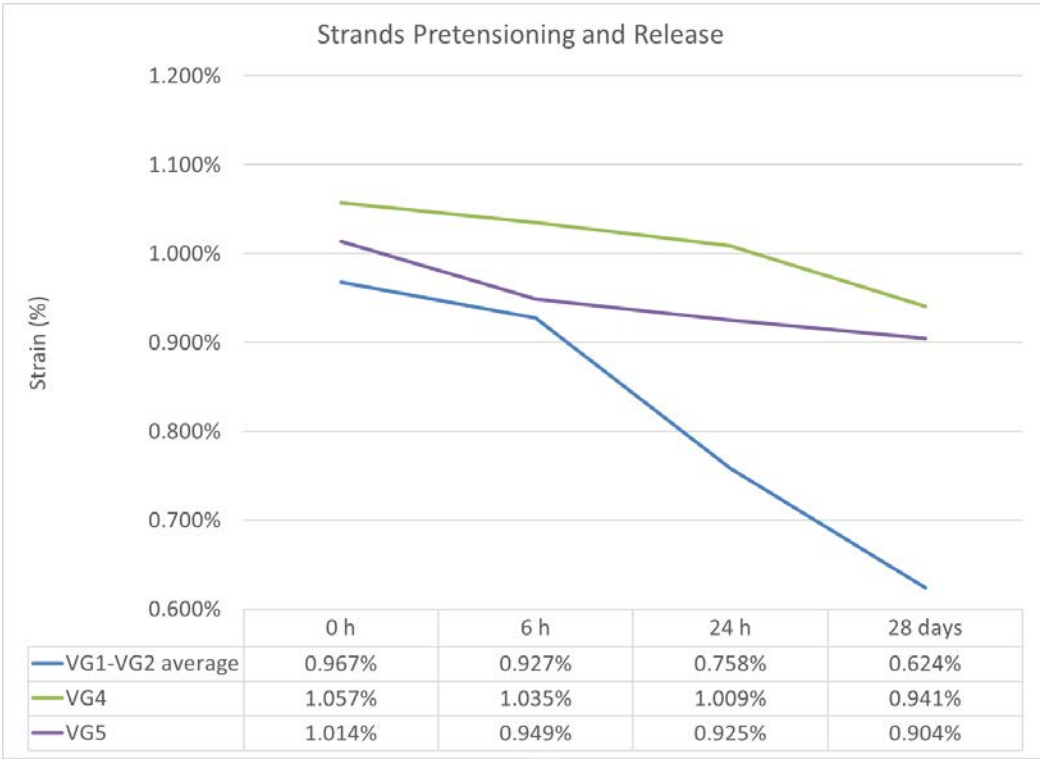

	0 h	6 h	24 h	28 days
VG1-VG2 average	0.967%	0.927%	0.758%	0.624%
VG4	1.057%	1.035%	1.009%	0.941%
VG5	1.014%	0.949%	0.925%	0.904%

Figure 7: Strains in tendons after tensioning, casting, releasing and curing phases

4. Load Test

4.1. Experimental Setup

In order to analyze the flexural response near service conditions, a load test was carried out on the instrumented DT girder before its installation on-site. The girder was loaded under a three-point-load setup, over the 66 ft effective span of the bridge model (Figure 8). Four rectangular hollow steel tubes placed over prismatic concrete elements were used as supports. A soft wood interface was provided between the supports and the girder bearing plates to help the levelling procedure and prevent stress concentration during the test. Three rectangular concrete blocks, each of them weighting 9 kip, were used to apply the intended load by mean of a crane (Figure 9).

The DT girder displacements were monitored using 10 analogic dial gauges, installed in correspondence of the two stems and located, along the girder length, as shown in Figure 10. Dial Gauges 1, 2, 3 and 4 were used to monitor the supports settlement and deformation; Dial Gauges 7 and 8 were aimed to measure the DT deflection at midspan whereas Dial Gauges 5, 6, 9, and 10, were positioned at quarter span.

Figure 8: DT girder loaded under a three-point-load setup

Figure 9: DT girder loading phase, dial gauges and supports

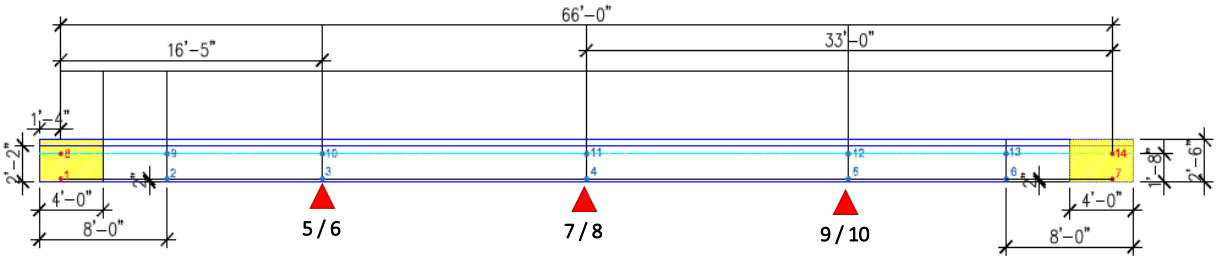

Figure 10: Dial gauges location

4.2. Loading cycles

For the purpose of this study, the service limit state was defined by the state at which the girders remained un-cracked. A total load of 27 kip was applied in three loading steps. The second and third concrete blocks were positioned on the DT girder, successively removed and then permanently repositioned on the girder midspan. The total load was finally applied over a 24 hours period. The loading and unloading phases took about 2 hours each. The dial gauges measurements were monitored at each load step.

A diagram of the adopted loading cycles is detailed in Figure 11.

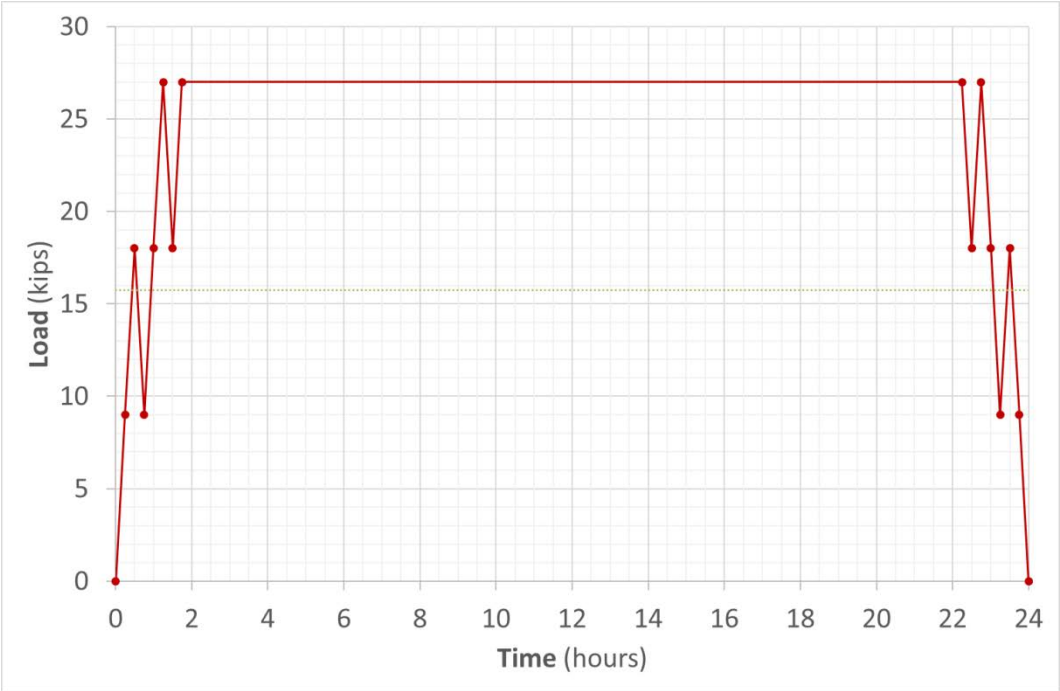

Figure 11: Loading cycles

4.3. Results and Discussion

Figure 12 shows the experimental load-deflection diagrams obtained during the 24 hours loading cycles. Figure 13 shows the deflection profile of the girder at the different loading phases. Figure 14 illustrates the measured strain profile at girder midspan cross-section. Finally, Figure 15 shows the strains measured in tendons at midspan from the tensioning phases up to the end of the load test. A theoretical prediction is reported in all diagrams.

The girder exhibited the elastic performance expected at the serviceability limit state, with no cracks being visually detected. Due to the 24 hours sustained 27-kip load, it was possible to observe

some creep/relaxation effects and compare them with theoretical predictions. These are computed by additively considering the long-term deformation caused by sustained loading on both concrete and CFRP tendons (Table 5).

The overnight additional deflection and the residual deflection after the load removal resulted in being equal to 0.12 in. and 0.14 in., respectively. These values are robustly in line with the expected values of 0.12 in. It is worth noting that, according to theoretical calculations, the most considerable contribution to overnight and residual deformation is given by concrete creep rather than CFRP relaxation.

Table 5

Deflection at DT Midspan	*Experimental Value*	*Theoretical Prediction*		
		Concrete	*CFCC*	*Total*
	(in.)	*(in.)*	*(in.)*	*(in.)*
Overnight	0.12	0.10	0.02	0.12
Residual	0.14	0.10	0.02	0.12

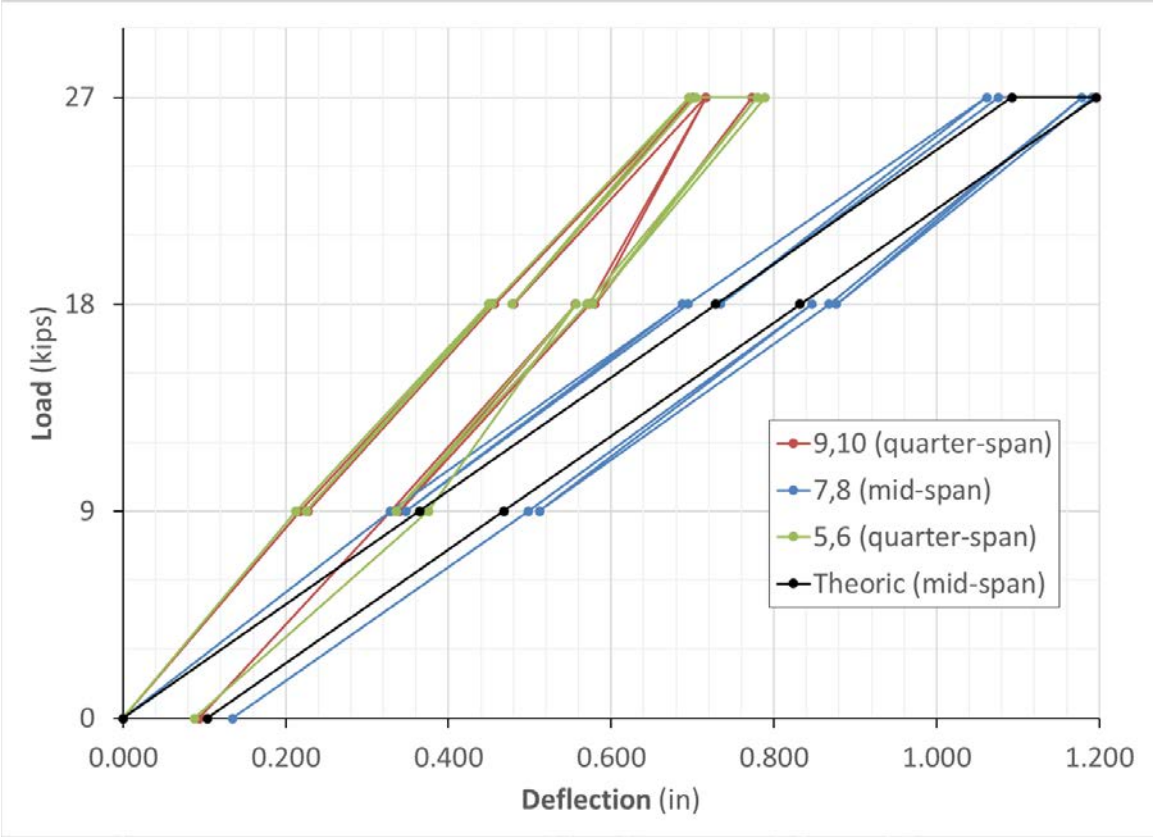

Figure 12: Load-deflection diagrams

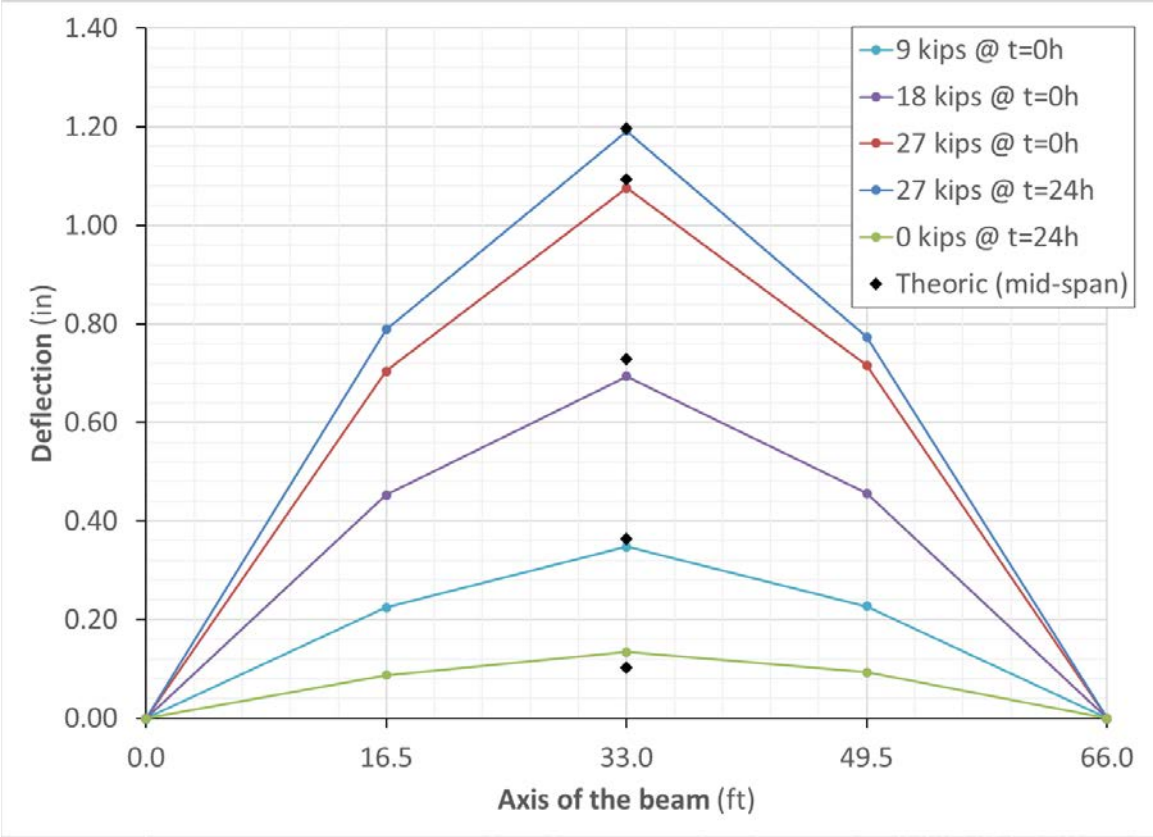

Figure 13: Deflection profile along the girder axis

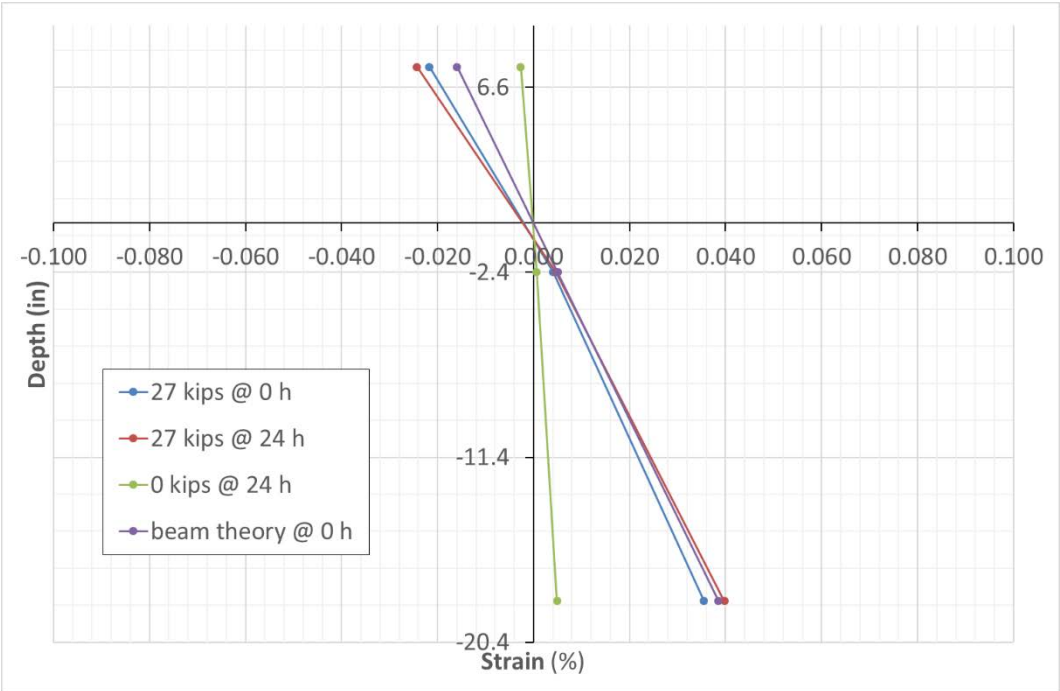

Figure 14: Measured strain profile at DT midspan

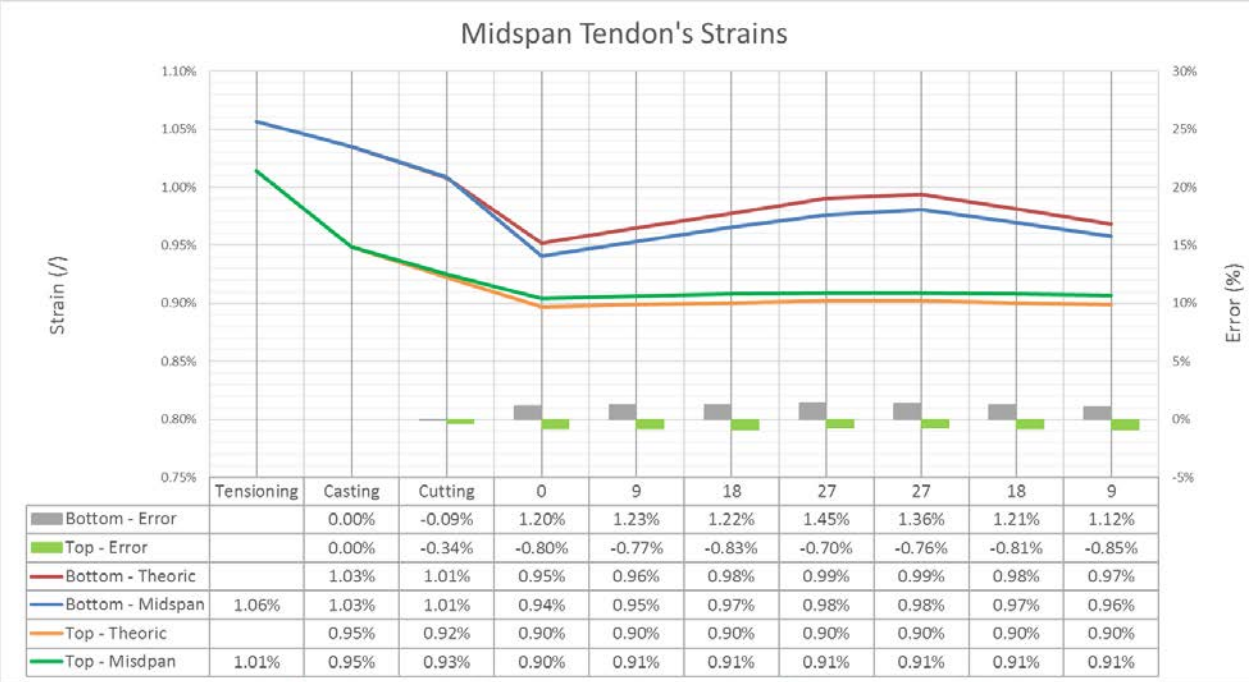

	Tensioning	Casting	Cutting	0	9	18	27	27	18	9
Bottom - Error		0.00%	-0.09%	1.20%	1.23%	1.22%	1.45%	1.36%	1.21%	1.12%
Top - Error		0.00%	-0.34%	-0.80%	-0.77%	-0.83%	-0.70%	-0.76%	-0.81%	-0.85%
Bottom - Theoric		1.03%	1.01%	0.95%	0.96%	0.98%	0.99%	0.99%	0.98%	0.97%
Bottom - Midspan	1.06%	1.03%	1.01%	0.94%	0.95%	0.97%	0.98%	0.98%	0.97%	0.96%
Top - Theoric		0.95%	0.92%	0.90%	0.90%	0.90%	0.90%	0.90%	0.90%	0.90%
Top - Misdpan	1.01%	0.95%	0.93%	0.90%	0.91%	0.91%	0.91%	0.91%	0.91%	0.91%

Figure 15: Tendon strain at midspan

5. Conclusions

The results of the study support the following conclusions:

- CFRP prestressing technology can be successfully employed in thin walled concrete sections without evident technological drawbacks;
- 68% of the guaranteed strength of tendons can be safely applied during the tensioning phase in order to fully exploit the mechanical properties of CFRP;
- Assumptions traditionally adopted for steel-PC can be substantially used when designing CFRP-PC sections; and,
- Concrete creep is affecting the loss of prestress more than CFRP relaxation.

6. References

ACI 440.4R-04 (2011), Prestressing Concrete Structures with FRP Tendons (Reapproved 2011), American Concrete Institute, Farmington Hills, MI

ACI 318-14 (2014), Building Code Requirements for Structural Concrete and Commentary, American Concrete Institute, Farmington Hills, MI

APPENDIX 3 – On-site Deflection Measurements

1. Monitoring Approach and Instrumentation

Deflection monitoring was carried on using a LEICA total station to read the position of reflective targets, properly applied over the side of one of the two double tee girders. LEICA targets used for the task measured 1.57 x 1.57 in. (40 x 40 mm).

Measurements were initially taken at the pre-cast yard and later on-site. In order to link the two series of readings in a global girder camber history, the initial measurements were referred to internal points over the girder length, always referenceable even after moving the girder itself. After the two girders positioning on-site, the target locations were measured from two different survey points:

- Point A at the left end of the instrumented girder, on the “parking lot” side
- Point B at the right end of the instrumented girder, on the “Wellness Center” building side

Three fixed reference points were positioned on the Wellness Center wall: one main reference and two backups (see Figure 1). Two points are visible from both the survey Points A and B, while the second backup can only be seen from Point A.

A total of 14 targets were placed on the girder side: seven at the girder bottom and seven at the centroid height. Of these, only 10 were visible on-site, because the ones at the girder ends were covered by formwork, even at the positioning time; this impediment, forced the use of the targets located at 8 ft. (2.44 m) from the girder ends as on-girder reference points for measurement correlations.

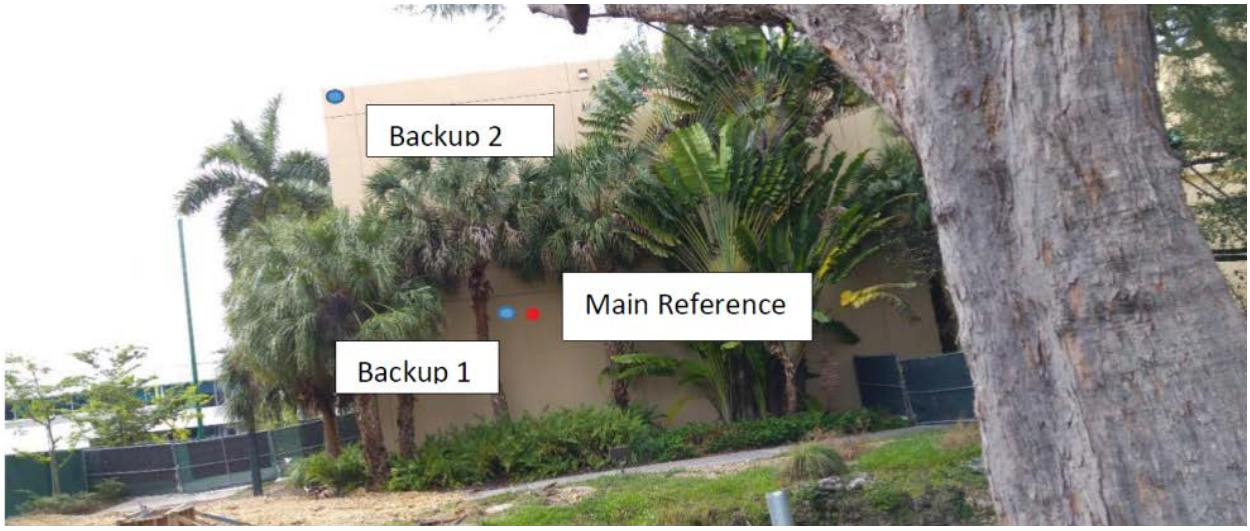

Figure 1: View from survey Point A

2. Targets

Targets (required for exactly pointing to a fixed reference over different reading sessions) were made of 1.57 x 1.57 in. (40 x 40 mm) reflective flat tape (Figure 2), for measurements up to 656 foot (200 m) of distance. For this type of targets, the total station requires a constant/offset of +1.35 in. (+34.4 mm) during the initial set up.

3. Total Station (LEICA TCR-805)

The total station is an electronic theodolite (transit) electronic/optical instrument for surveying integrated with an electronic distance meter (EDM) to read slopes and distances from the instrument to a particular point, a target, in this case (see Figure 2).

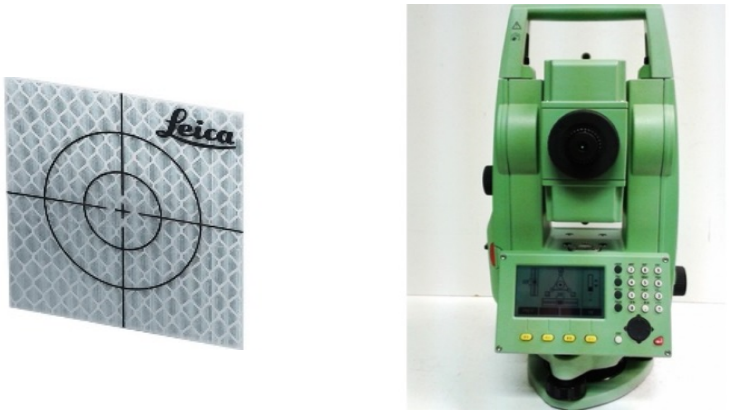

Figure 2: LEICA target and total station

4. Plan and Profile Views

Figures 3 and 4 show, respectively, the on-site plan view of the area where the bridge was built, and the profile view with the location of every target initially installed onto the instrumented girder.

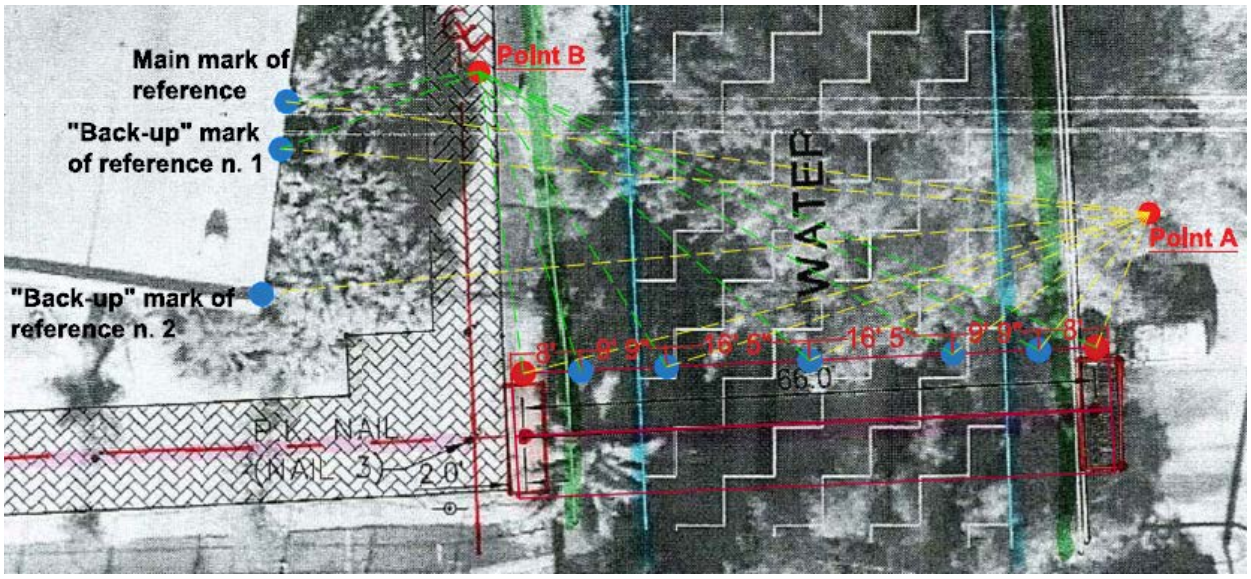

Figure 3: On-site plan view

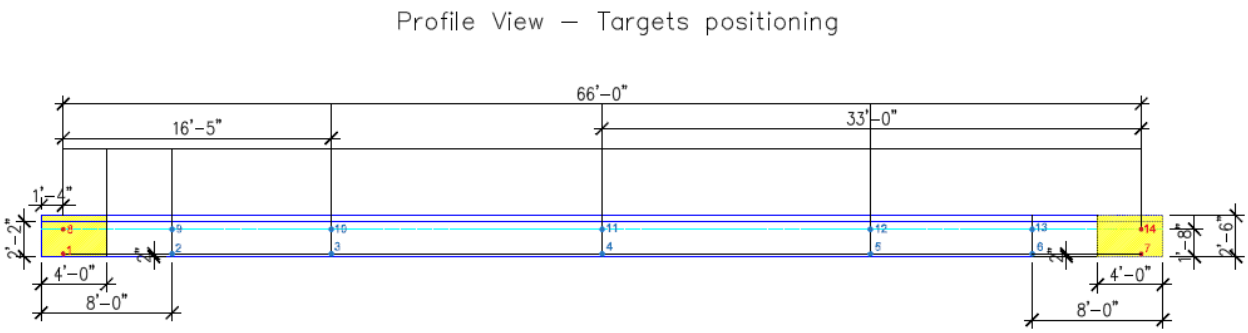

Figure 4: Side view & target locations

Figure 5 shows a photograph of the girder stem with targets visible from the survey Point A.

Figure 5: Targets view from Point A

4. Surveying Procedure

Tripod Setup

i. Point A and Point B are fixed points recognizable by a thick boron fiber nail drilled into the ground, for Point A, and by an indelible orange circle, for Point B, respectively. Start survey from Point A and subsequently repeat the procedure at Point B.

ii. Level the total station with accuracy - tripod legs should be equally spaced, tripod head should be approximately leveled and the head should be directly over the survey point.

iii. Observe each target in the optical plummet and center the target by loosening the centering screw and sliding the entire instrument.

iv. After re-tightening the centering screw, check to make sure the plate level bubble is leveled in the three directions.

Total Station Setup

i. Ensure that the all the measuring units of the total station are in US customary and the instrument is properly set to read each target [in the EDM settings, select the required type: 1.57 x 1.57 in. (40 x 40 mm)].

ii. Use a tape measure to determine the height of the instrument. Position the tape measure orthogonal and vertical to the terrain, then complete the survey report model (see Figure 6) with the measured instrument height.

DATE: OPERATORS:

SURVEY ON "HECTH" BRIDGE'S GIRDER

FROM POINT A

East side-Temperature: ABOVE: °C	**East side-Temperature:** BELOW: °C
West side-Temperature: ABOVE: °C	**West side-Temperature:** BELOW: °C
mid-span Temperature: ABOVE: °C	**mid-span Temperature:** BELOW: °C

MAIN REFERRING POINT	
TOTAL STATION	TARGET ON THE "HERBERT" WELLNESS CENTER BUILDING
h_i = ft	h_1 = ft

BACK-UP REFERRING POINT 1	
TOTAL STATION	TARGET ON THE "HERBERT" WELLNESS CENTER BUILDING
h_i = ft	h_1 = ft

BACK-UP REFERRING POINT 2 (UPPER POINT)	
TOTAL STATION	TARGET ON THE "HERBERT" WELLNESS CENTER BUILDING
h_i = ft	h_1 = ft

POINT A	
TOTAL STATION	TARGETS ON THE GIRDER
h_i = ft	h_1 = ft
	h_2 = ft
	h_3 = ft
	h_4 = ft
	h_5 = ft
	h_6 = ft
	h_7 = ft
	h_8 = ft
	h_9 = ft
	h_{10} = ft
	h_{11} = ft
	h_{12} = ft
	h_{13} = ft
	h_{14} = ft

Figure 6: survey report model

iii. Since the total station is an accurate-precision system sensitive to external conditions such as the effect of the sun, it is recommended to wait at least 15-20 minutes so that the total station can adjust to the external temperature. In the meanwhile, record temperature measurements with the infrared thermometer: check the air temperature and the temperature on the edges and at mid-span of the instrumented PC girder extrados and intrados. At the intrados, check both the bottom of the flange and the bottom of the stem, at the extrados check both the top of the flange and the top of the curb.

Taking the Readings

i. Take the measurements of the main reference target (Wellness Center) and the backup Points 1 and 2.

ii. Point the total station to the bridge and measure every target located on the instrumented girder at stem bottom (numbered from 2 to 6) and at centroid height (numbered from 9 to 13) for a total of 10 targets.
iii. Complete the survey report with every taken value.
iv. Repeat the process from the survey Point B.

5. On-site Load test

An on-site load test was performed after the deck was cast and the curbs and shoulders completed. To perform this load test, a pick-up truck with the following characteristics was used:

- Total length and width: 248 and 80 in. (6.3 and 2 m)
- Loaded front and rear axles: 4.36 and 7.72 kip (19.4 and 34.3 kN)

The load test was conducted in two parts: as a maximum moment test and a maximum shear test. For the first one, the truck was longitudinally centered facing the parking lot in order to measure strains and deflections. In this way, the front axle of the truck was positioned at a distance of 117 in. (3 m) from the left end (parking lot), while the rear axle was positioned at a distance of 275 in. (7 m) again from the left end. The total weight of the vehicle and its cargo was 12.08 kip (54 kN), with the heavier axle weighing 7.72 kip (34 kN). The mid-span moment generated by the vehicle for load position one (maximum moment) and including self-weight (two girders, decks, and curbs) was equal to 1,418 kip·ft (1922 kN·m), while the shear at the support for load position two (maximum shear) including self-weight was 85 kip (380 kN). The bridge is designed for a distributed live load of 100 psf (4.8 kN/m^2), which will result in a service maximum moment of 1,894 kip·ft (2,568 kN·m) and a maximum shear of 115 kip (511 kN). Figure 7 shows the truck moving over the bridge.

Figure 7: On-site load test

6. Target Replacement

Because the bridge had to be painted for aesthetical reasons, the targets were covered and had to be replaced. Again, thanks to the use of the total station and the fixed reference points on the Wellness Center, it was possible to conduct this operation with high precision. The performed procedure is reported hereinafter.

H_1, H_2 = reference point heights measured before and after replacement
h_1, h_2 = target heights measured before and after replacement
$\Delta\varepsilon_1$, $\Delta\varepsilon_2$ = errors intrinsically present in the measures

Figure 8 is a sketch of the situation before and after the targets replacement showing that the only unknown is h_2, the height where the target has to be positioned.

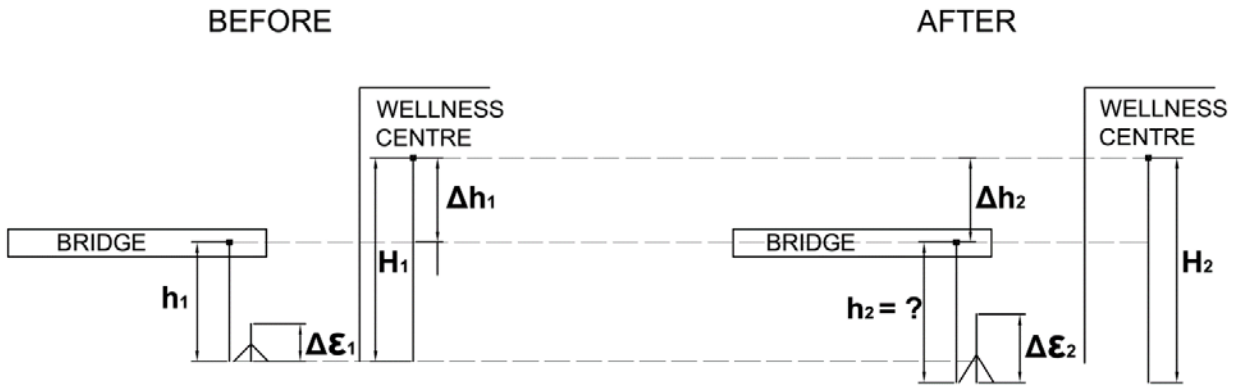

Figure 8: Before and after targets replacing

On-site measures taken at two different times are always different because of intrinsic errors resulting from tripod height, air refraction and incidence angle. Thus, Δh_1 and Δh_2 can be defined as:

$$\Delta h_1 = (H_1+\Delta\varepsilon_1)-(h_1+\Delta\varepsilon_2) = H_1-h_1$$
$$\Delta h_2 = (H_2+\Delta\varepsilon_2)-(h_2+\Delta\varepsilon_2) = H_2-h_2$$

By imposing:

$$\Delta h_1 = \Delta h_2$$

And substituting for Δh_2, it results that:

$$(h_2+\Delta\varepsilon_2) = (H_2+\Delta\varepsilon_2)-\Delta h_2$$
$$(h_2+\Delta\varepsilon_2) = (H_2+\Delta\varepsilon_2)-\Delta h_1$$

Assuming that heights measured at the same time from the same setup come with the same error, the expression above can be re-written as:

$$h_2 = H_2-\Delta h_1 = H_2-(H_1-h_1)$$
$$h_2 = h_1-(H_2-H_1)$$

Knowing the targets location before replacement and the difference in the reference point heights, the total station can point to the location where each new target has to be placed.

Errors in the procedure always occur, but the differences in the readings before and after can be resolved correcting the after-readings by such a value. Five new targets are now located on the

instrumented girder, at centroid height. These targets are numbered 9, 10, 11, 12 and 13 on the profile view of Figure 4.

7. Data Analysis

A survey (from Points A and B) was conducted before casting the deck. Another was conducted after the deck was cast, and a third one occurred after the curbs were cast. Having a set of three measures, it was possible to compute the standard deviation and evaluate the best way to handle the data.

The measures were referred to each reference point and to the instrument height. Comparing the standard deviation, the main reference point resulted the less scattered. Two options were taken into consideration:

- Consider all measures (3 from A + 3 from B = 6) as independent STD = 0.300 in. (7.6 mm)
- Consider the average of the three measures from A and separately from B as single measures STD = 0.176 in. (4.5 mm)

It is clear that the second option is preferable. In this report, only the survey of the five targets at the centroid height is given as this represents the neutral axis of the girder. The average of the measures taken before the deck casting was considered as the "on-site-zero" and the reference for computing further increments.

8. Thermal Deflection

A thermal gradient over the girder causes a differential thermal expansion that results in displacements. These displacements must be subtracted from the field measurements taken at different times and different temperatures in order to be able to compare results. This can be accomplished by computing an equivalent thermal moment as follows:

$$\chi_T = \frac{\alpha\, \Delta T}{H}$$
$$M_T = \chi_T\, EJ$$

The deflection at any point along the girder can be computed according to the following deflection expression for a simply supported span under a constant bending moment.

$$\delta_T(z) = \frac{1}{2}\frac{M_T L^2}{EJ}\left[\left(\frac{z}{L}\right) - \left(\frac{z}{L}\right)^2\right]$$

9. Results

In this section, the results of the field survey during the bridge construction phases are compared to the ones obtained immediately after the girders were installed. The following figures show the change in camber.

- Girder camber. In Figure 9, five curves are shown starting from the one recorded at the time of girder installation through the one during the load test with truck positioned to generate the maximum moment. Plotting the net camber data over the girder length, a consistent symmetric shape can be clearly identified as well as a consistent deflection increment (i.e., reduction in camber) at increasing load.

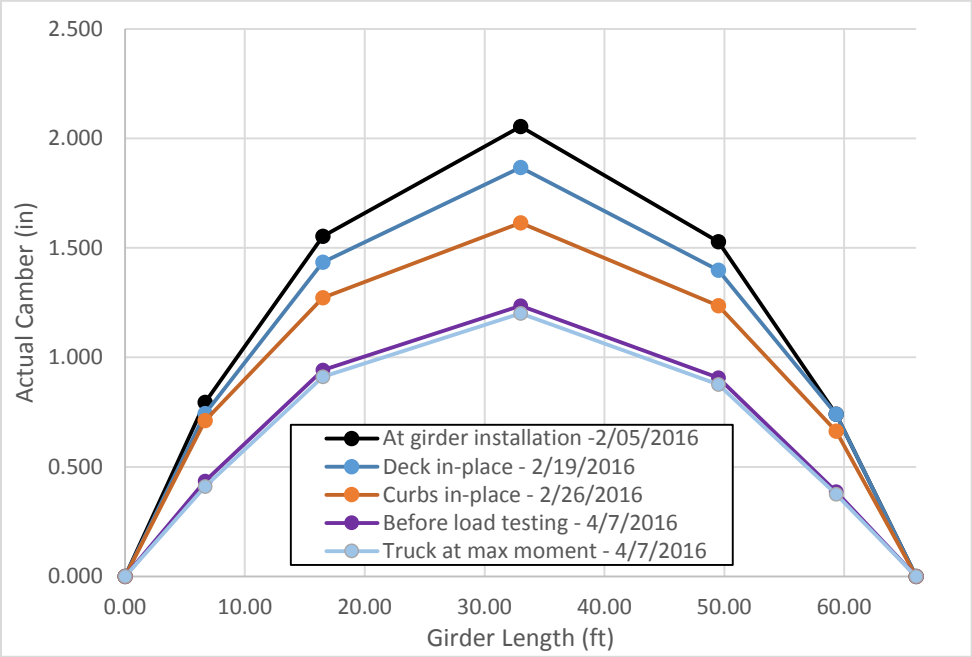

Figure 9: Camber values measured at centroid-height targets

- On-site load test. Figure 10 shows the results obtained from the truck positioned at maximum shear and at maximum moment locations. For the maximum shear test, the camber trend line does not vary from the reference line (unloaded condition), whereas the trend line for the maximum moment test shows a slight reduction in camber.

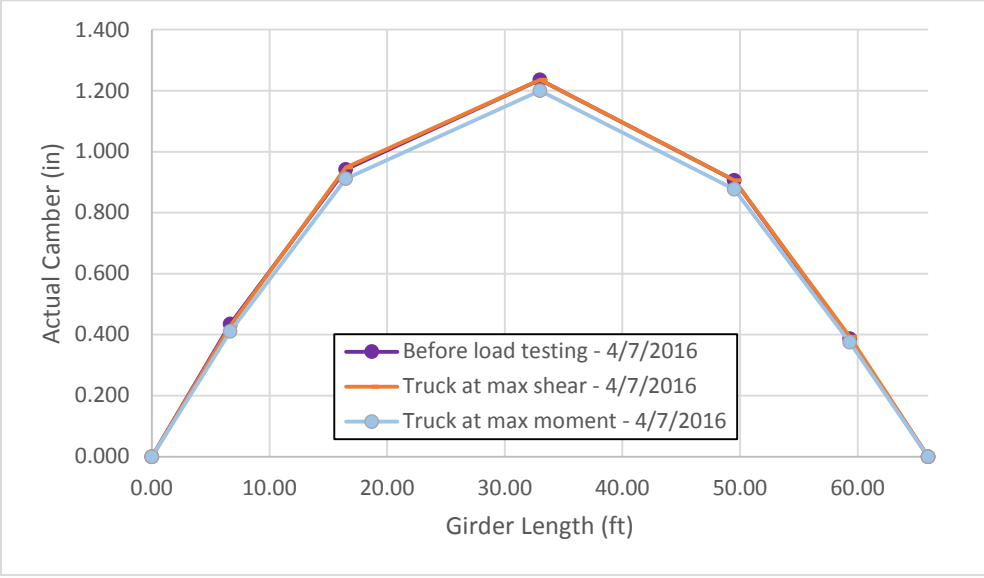

Figure 10: Camber values for on-site load test

Figure 11 shows the deflection increments as a result of loading rather than the reduction in camber. The reference line (zero line) is the deflection at the time of girder installation. An almost perfectly symmetric shape of the deflections increments is apparent.

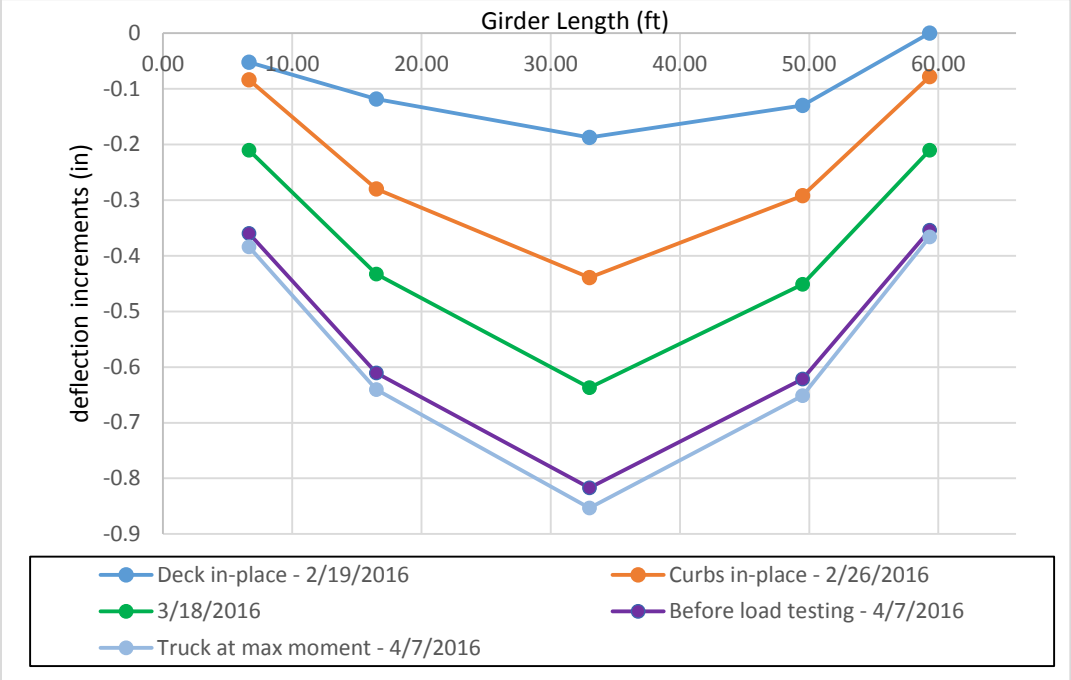

Figure 11: Deflection from initial on-site camber - increments – refined

Figure 12 shows the theoretical/experimental camber values over the girder load and construction history up to the end of April 2016.

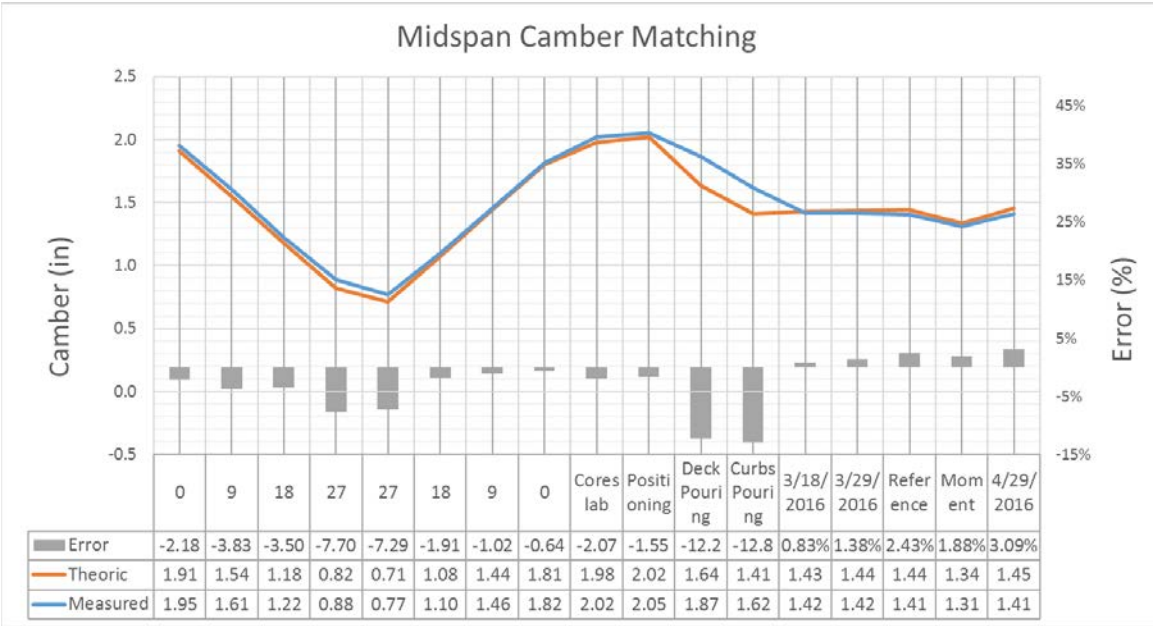

	0	9	18	27	27	18	9	0	Cores lab	Positioning	Deck Pouring	Curbs Pouring	3/18/2016	3/29/2016	Reference	Moment	4/29/2016
Error	-2.18	-3.83	-3.50	-7.70	-7.29	-1.91	-1.02	-0.64	-2.07	-1.55	-12.2	-12.8	0.83%	1.38%	2.43%	1.88%	3.09%
Theoric	1.91	1.54	1.18	0.82	0.71	1.08	1.44	1.81	1.98	2.02	1.64	1.41	1.43	1.44	1.44	1.34	1.45
Measured	1.95	1.61	1.22	0.88	0.77	1.10	1.46	1.82	2.02	2.05	1.87	1.62	1.42	1.42	1.41	1.31	1.41

Figure 12: Camber values over the girder load history

10. Conclusions

- A consistent method to obtain deflection readings with high precision was developed using the total station. This method will be a useful tool in future years for deflection monitoring of the bridge.
- Deflections accounting for temperature variations recorded on-site were matched with analytical predictions confirming the reliability of the adopted theoretical approach.